# Enhanced densification of Ti–6Al–4V powders by transformation-mismatch plasticity

Bing Ye [a], Marc R. Matsen [b], David C. Dunand [a,*]

[a] *Department of Materials Science and Engineering, Northwestern University, Evanston, IL 60208, USA*
[b] *Boeing Research & Technology, The Boeing Company, Seattle, WA 98124, USA*

## Abstract

The densification kinetics of Ti–6Al–4V powders with spherical or angular shapes are compared in uniaxial die pressing experiments between isothermal conditions (at 1020 °C, in the β-field, where deformation occurs by creep) and thermal cycling (between 860 and 1020 °C, within the range of the α–β phase transformation of the alloy, where transformation-mismatch plasticity is activated). Densification kinetics are only moderately affected by powder shape, but are markedly faster under thermal cycling than under isothermal conditions, as expected from the higher deformation rate achieved under transformation-mismatch plasticity conditions as compared to creep conditions. The densification curves for both creep and mismatch plasticity deformation mechanisms are successfully modeled for various applied stresses and for partial cycling, when transformation is incomplete. Tensile properties of specimens fully densified under thermal cycling conditions are similar to literature values from Ti–6Al–4V densified by isothermal hot isostatic pressing.
© 2010 Acta Materialia Inc. Published by Elsevier Ltd. All rights reserved.

*Keywords:* Powder consolidation; Hot pressing; Titanium; Phase transformations; Superplasticity

## 1. Introduction

The alloy Ti–6Al–4V provides a combination of high static and fatigue strength, low density and excellent corrosion resistance, making it widely used in the aerospace and biomedical industries. Powder metallurgy is often used to create complex Ti–6Al–4V objects because it is a near-net shape process, which can reduce cost as compared to the traditional casting/forging/machining route [1]. To reach full density, however, often requires the use of hot isostatic pressing (HIP). Vacuum hot-pressing of powders in dies is typically simpler and less expensive than HIP, but the lower pressures achievable reduce the densification rates, leaving residual porosities after the operation or requiring prohibitively long pressing times.

The initial stage of metal powder densification at elevated temperature is controlled by the time-dependent deformation (e.g. by diffusional or dislocation creep) of individual powders in contact with each other [2]. An alternate deformation mechanism is transformation-mismatch plasticity, which has been studied extensively in bulk metals and alloys, in particular commercial-purity titanium (CP-Ti) [3–11] and Ti–6Al–4V [8,12–14], as well as their composites [14–17] and foams [18–20]. When allotropic materials are subjected to a uniaxial stress while the temperature is repeatedly cycled, the internal transformation mismatch stresses are biased by the external stress [11]. This leads to a reduction in flow stress as compared to isothermal deformation, an increase in average strain rate sensitivity towards Newtonian deformation and an increase in elongations to fracture, which are characteristic of superplasticity [11,12]. The decreased flow stress and increased strain rate sensitivity observed in bulk samples can be used for improving powder densification kinetics, as shown by various researchers [21–23] for iron-based powders densified during thermal cycling. This approach has also been explored for titanium. Leriche et al. [24]

* Corresponding author. Tel.: +1 847 491 5370.
  *E-mail address:* dunand@northwestern.edu (D.C. Dunand).

measured the kinetics of hot-pressing for Ti–6Al–4V powders subjected to a relatively high pressure of 30 MPa. Densities above 99% were achieved both under cycling between the α–β and the β-range (800–1040 °C) and isothermal conditions in the β-range (1040 °C), while the isothermal densification in the α-range gave significantly lower densities. The authors calculated that the contribution to densification from transformation-mismatch plasticity during the first and second cycles was larger than the contribution of creep. Schuh et al. [4] carried out uniaxial hot-pressing densification of CP-Ti powders isothermally at 980 °C (in the β-field of CP-Ti) and during thermal cycling between 860 and 980 °C (about the α/β allotropic temperature of CP-Ti) for stresses of 1–3 MPa. Transformation-mismatch plasticity accelerated markedly the kinetics of densification, despite a lower average temperature during cycling. Continuum models of powder densification gave accurate predictions of powder densification behavior under both isothermal and thermal cycling conditions, when using the appropriate deformation mechanism (isothermal creep and transformation-mismatch plasticity, respectively).

In the present article, we show that transformation-mismatch plasticity by thermal cycling can significantly enhance the uniaxial hot-pressing densification kinetics of Ti–6Al–4V prealloyed powders as compared to isothermal consolidation. Densification curves are measured for applied pressures between 3 and 30 MPa for two powders with different shapes, and are modeled using the same continuum approach used previously for CP-Ti [4], modified to take into account the much wider range of transformation temperatures prevalent in Ti–6Al–4V. Furthermore, the microstructure and tensile properties of the Ti–6Al–4V densified by thermal cycling are examined and compared to those for HIP-densified material.

## 2. Experimental procedures

### 2.1. Materials

Two types of Ti–6Al–4V powders were investigated: (i) spherical powders produced by the plasma rotating electrode process (PREP), supplied by Starmet Corp. and (ii) angular shaped powders produced by hydrogenation/dehydrogenation (HDH), supplied by Reading Alloys, Inc. The PREP Ti–6Al–4V Extra Low Interstitial (ELI) powders exhibited a particle size of ∼80 μm (Fig. 1) and the following composition (in wt.%): 6.07% Al, 3.81% V, 0.192% O, 0.18% Fe, 0.02% C, 0.02% Si (ASTM F136). The HDH powders were angular in shape with typical dimensions of 100 × 200 μm (Fig. 2) and the following composition (in wt.%): 5.50–6.75% Al, 3.50–4.50% V, 0.30% Fe, 0.20% O, 0.08% C, 0.05% N and 0.015% H (ASTM F 1580-1).

### 2.2. Powder consolidation

A custom vacuum hot press apparatus was used, similar to that described in Ref. [4]. The powder was poured and manually tapped in a cylindrical graphite die coated with boron nitride, with inner and outer diameters of 19.1 and 63.5 mm and a height of 19.1 mm. A stainless steel piston transmitted the uniaxial load to the powders in the die cavity, which were contained at the other end of the die by a stainless steel base. The total mass of powder was $6.41 \pm 0.005$ g, equivalent to a final height of 5.0 mm after full densification. Both piston and base were separated from the powder by two 125 μm thick stainless steel foils coated with boron nitride. The powder temperature was monitored by a K-type thermocouple in contact with the center of the stainless steel piston. This formed the assembly for powder consolidation.

A uniaxial compressive load from an universal testing machine was transmitted to the assembly by two quartz columns through two pistons outfitted with O-rings for both low friction and leak-free motion between the pistons and the quartz tubing wall separating the evacuated assembly from the atmosphere. During induction heating from ambient to densification temperature with a heating rate ∼1 K s$^{-1}$, the powders were subjected to a small 0.4 MPa compressive stress (defined here and in the following as the applied load divided by the cross-sectional area of the 19.1 mm diameter pistons). This slow heating rate was used to permit thorough degassing and to achieve uniform temperature in the assembly, given the relatively low thermal conductivity of Ti–6Al–4V powders. In the isothermal experiments, the densification stress was applied to the powders when the temperature reached 1020 °C (in the β-field of Ti–6Al–4V) and the stress and temperature were maintained constant throughout the experiment. In the thermal cycling experiments, the densification stress was applied when the temperature reached 850 °C, and then the stress remained constant while the temperature was cycled between 860 and 1020 °C with heating time of 96 s and cooling time of 95 s under constant heating power. At these lower and upper temperatures, the volume fraction of β phase is 22% and 100%, respectively [12]. A vacuum level of at least $5 \times 10^{-5}$ Torr (6.7 mPa) was maintained throughout the experiment. The temperature was recorded every 2 s, together with the piston displacement measured at the cross-head by a displacement transducer with an accuracy of $\pm 3$ μm. After the experiments, the sample was cooled in vacuum to room temperature within 2 h. The density of the sample was measured by the Archimedes method (correcting for the presence of vacuum grease used to seal any open pore), assuming a density of 4.43 g cm$^{-3}$ for bulk Ti–6Al–4V [25]. The relative density during the densification experiment was then calculated using the measured final density and the piston displacement data.

Metallographic preparation was conducted on mounted samples after cutting with a diamond saw, using an automatic grinder polisher with 9 and 1 μm diamond suspensions, and final polishing with 0.05 μm colloidal silica. After thorough cleaning, the samples were etched for 15 s with Kroll's reagent (2 ml HF and 6 ml HNO$_3$ in 100 ml distilled water) before observation by optical microscopy.
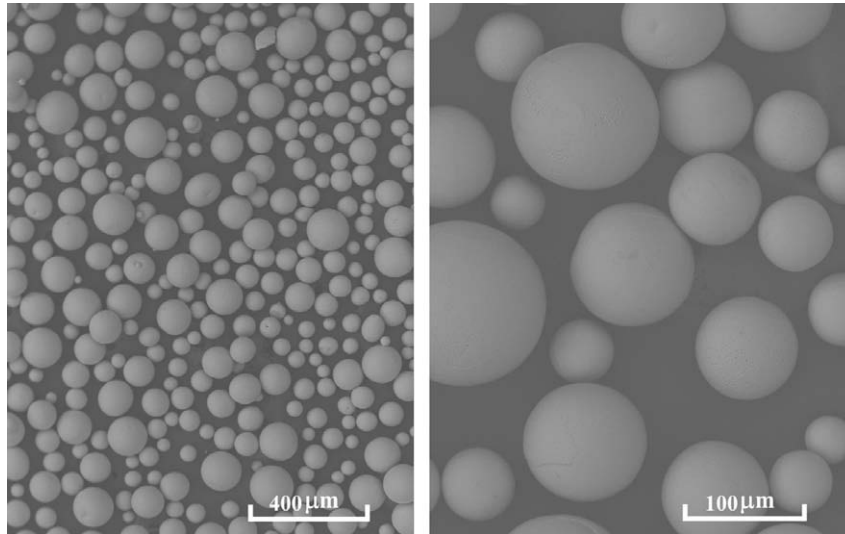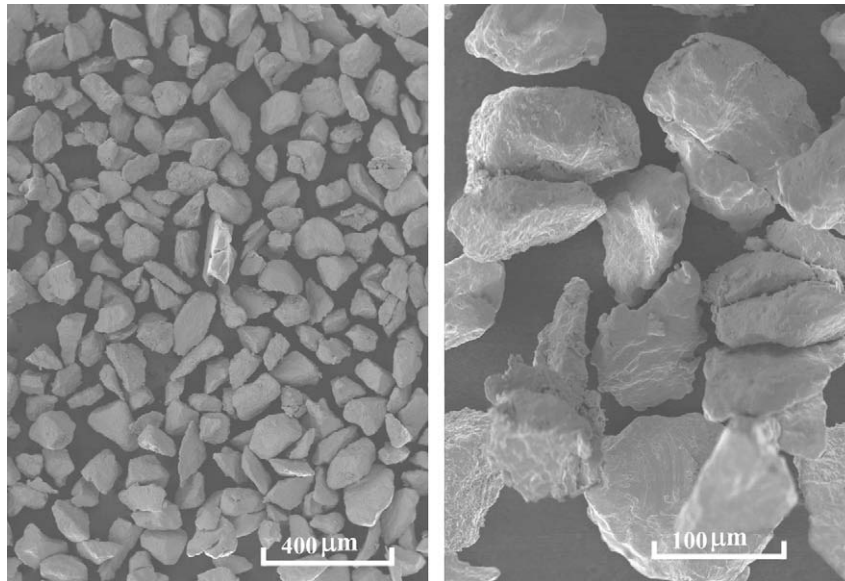
Fig. 1. SEM images of spherical PREP powders.



Fig. 2. SEM images of angular HDH powders.

## 2.3. Tensile testing

A TZM molybdenum die with 63.5 mm outer diameter was used to densify a rectangular prism of Ti–6Al–4V with dimensions of $38.1 \times 25.4 \times 19$ mm$^3$. Densification occurred under a stress of 15 MPa with thermal cycling between 860 and 1010 °C for 2 h. Final relative density was >99.9%. Flat dog-bone tensile specimens (12.7 mm gauge length, 3.2 mm gage width and 3.2 mm gage thickness) were created by electrical discharge machining. Two tensile specimens were mill-annealed at 700 °C for 2 h (at the lower boundary of the mill annealing temperature range of 700–750 °C) [25] in a vacuum furnace and polished with 9 μm diamond suspension before conducting tensile testing at a strain rate of $10^{-3}$ s$^{-1}$ with strain measured by extensometry.

## 3. Results

### 3.1. Microstructure and mechanical properties

The etched microstructures of the densified Ti–6Al–4V samples are shown in Figs. 3 and 4 for samples consolidated by thermal cycling (for 40 min at 15 MPa) from PREP and HDH powders, respectively. The residual porosities were $0.60 \pm 0.05\%$ and $0.50 \pm 0.05\%$, respectively, and, as expected, very few pores are visible in the micrographs. A Widmanstätten or "basket weave" structure is visible, which is typical of slow-cooled Ti–6Al–4V. The two mill-annealed specimens machined from a fully densified Ti–6Al–4V HDH sample exhibited the following tensile properties: $865 \pm 5$ MPa for yield strength; $940 \pm 5$ MPa for
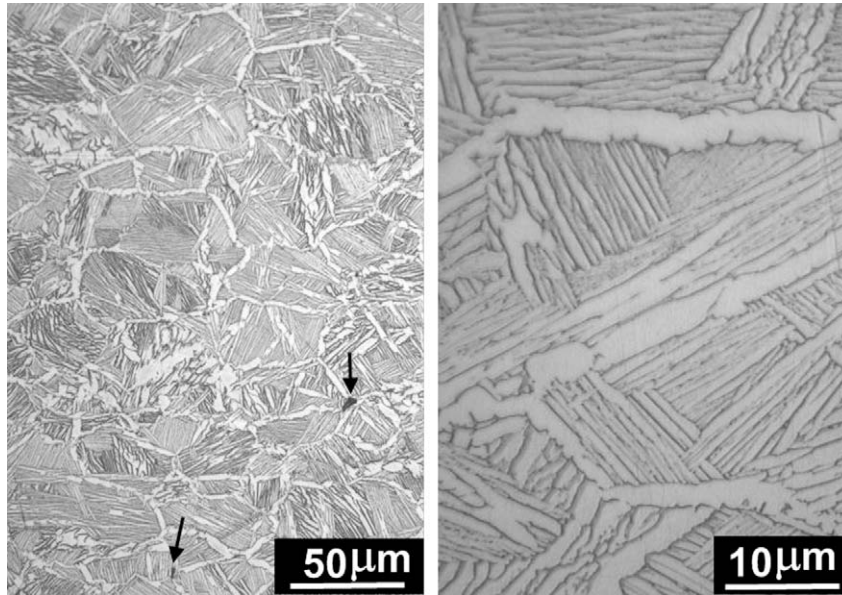
Fig. 3. Etched optical micrographs of sample densified from PREP powders after thermal cycling (40 min and 15 MPa). Two pores are marked by arrows.
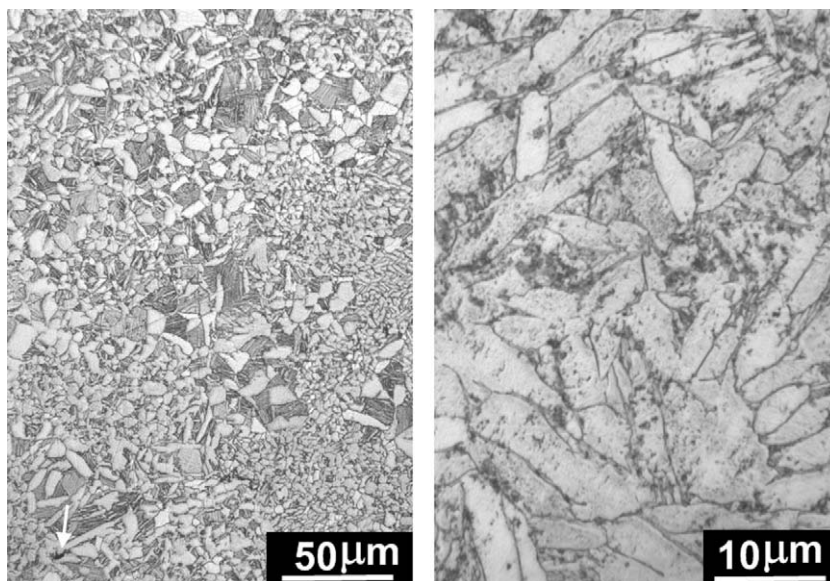


Fig. 4. Etched optical micrographs of sample densified from HDH powders after thermal cycling (40 min and 15 MPa) consolidation. A pore is marked by the arrow.

ultimate strength; $18 \pm 2\%$ for elongation to fracture. These values are similar to those reported for Ti–6Al–4V densified by conventional HIP of ELI powders [25], confirming the near full densification and low oxygen content of our specimens.

### 3.2. Isothermal and thermal cycling densification

Densification curves (relative density vs. time) for both angular HDH Ti–6Al–4V and spherical PREP Ti–6Al–4V powders densified isothermally at 1020 °C are shown in Fig. 5a and b for a wide range of applied uniaxial pressure (3–30 MPa). The densification rate decreases steadily with time (or density), and increasing the stress increases the density and densification rate at a given time. Full densification is not achieved for PREP powders in technologically relevant times when the applied pressure is below 15 MPa. This is typical for isothermal powder densification and is reflected by the much higher pressures (of the order of 100 MPa) used during commercial HIP densification to achieve full density in Ti–6Al–4V. Direct comparison between the densification curves of Fig. 5a and b for HDH and PREP powders is complicated by the difference in initial relative density: for the manual tapping used here, the spherical PREP powders (initial relative density ~55%) pack better than the angular HDH powders (initial relative density ~47%).
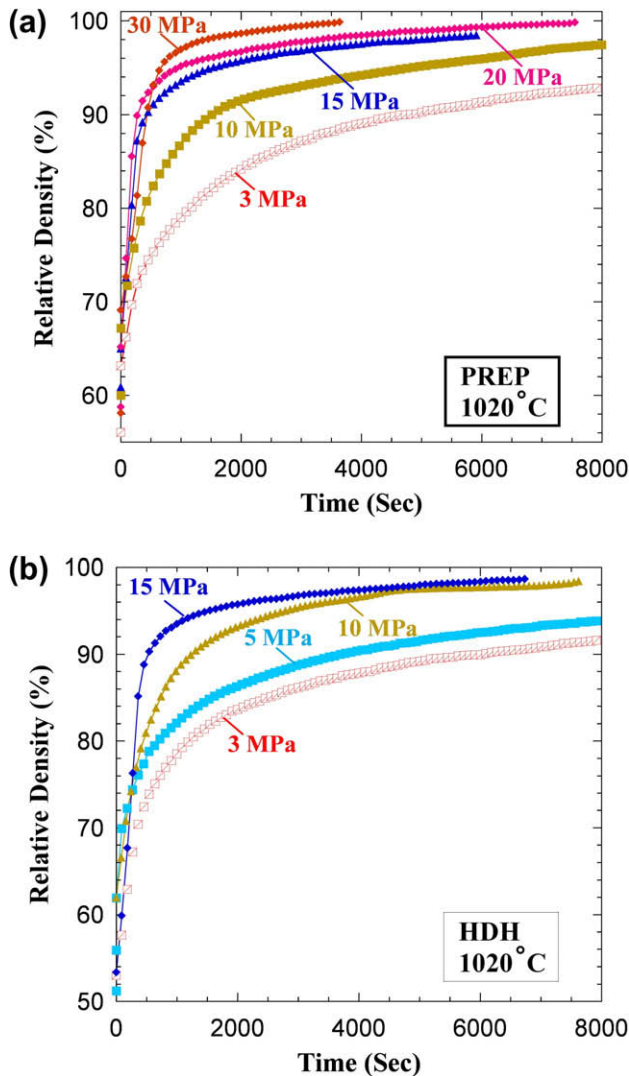
Fig. 5. Densification curves conducted isothermally at 1020 °C for various stresses: (a) PREP powders and (b) HDH powders.

Fig. 6. Densification curves for HDH powders performed under isothermal and thermal cycling conditions under a stress of: (a) 5 MPa and (b) 10 MPa.

A comparison of densification kinetics for HDH powders between isothermal and thermal cycling conditions is shown in Fig. 6a and b under stresses of 5 and 10 MPa, respectively. For a stress of 5 MPa (Fig. 6a), the densification behavior is similar for relative density below ~80%. Beyond that density, the curves diverge, with thermal cycling conditions achieving near full densification (~99.4%) after 2 h of pressing, while isothermal conditions result in a density of ~92% after ~3 h. This improvement occurs despite the average temperature for the cycling conditions (940 °C) being significantly lower than the isothermal temperature (1020 °C). In Fig. 6a, two isothermal curves are shown to illustrate the level of reproducibility between independent experiments: differences may be due to variation in initial powder packing and friction between powder and graphite die, although the inner wall of the graphite die was coated with boron nitride to enhance lubrication.

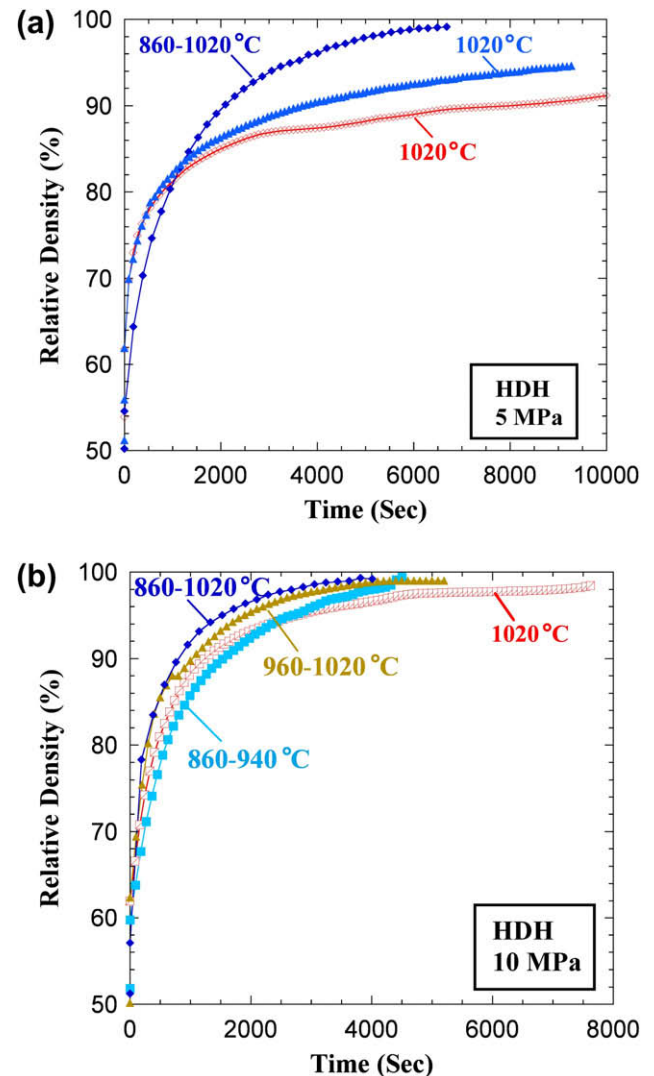A similar improvement in densification due to thermal cycling is observed at 10 MPa (Fig. 6b). Transformation-mismatch plasticity leading to this enhancement in densification kinetics during thermal cycling is expected to take place over most of the cycling temperature range (860–1020 °C), since Ti–6Al–4V has a continuous phase transformation region between 600 and 1000 °C [12]. Partial cycling, i.e. 860–940 and 960–1020 °C using the same power input (i.e. heating and cooling rates) but reduced cycling periods of 90 and 100 s, respectively, leads to somewhat reduced densification kinetics and longer time to achieve full densification, as compared to full cycling (860–1020 °C with 191 s period), as shown in Fig. 6b. These times are however much shorter than for the isothermal conditions at 1020 °C, despite the lower average temperature (900 °C for 860–940 °C cycling and 990 °C for 960–1020 °C).

The effect of applied stress on densification kinetics under full thermal cycling (860–1020 °C) is shown for spherical PREP powders (Fig. 7a) and angular HDH powders (Fig. 7b). The densification kinetics is enhanced with increasing stress, as for isothermal densification (Fig. 5a
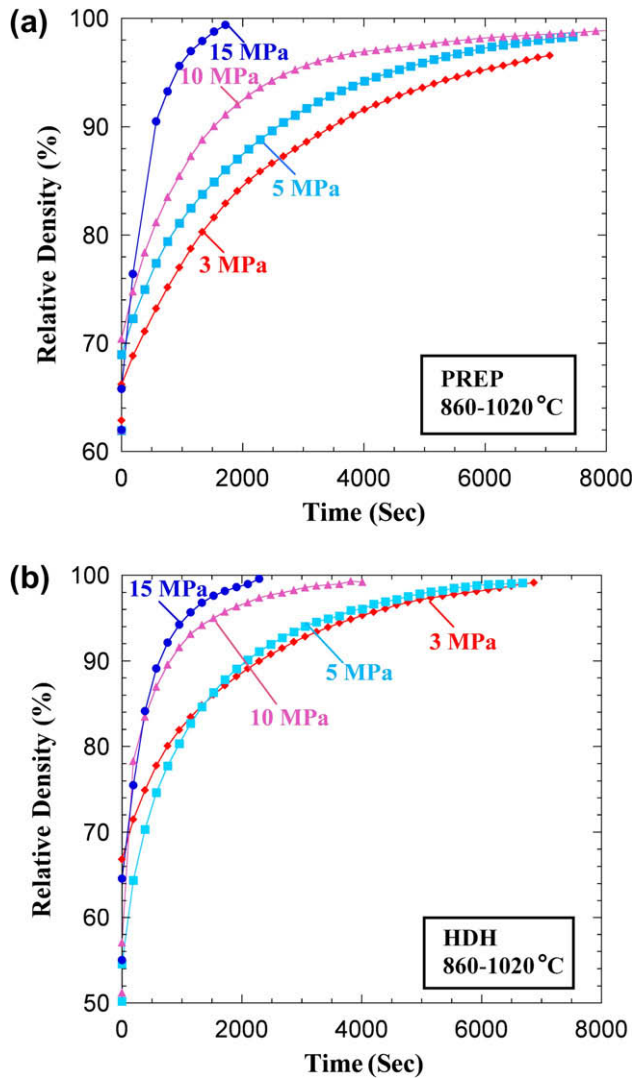
Fig. 7. Densification curves for various stresses performed under thermal cycling conditions for: (a) PREP powders and (b) HDH powders.

and b). Comparison of densification behavior between spherical PREP powders and angular HDH Ti–6Al–4V powders at a given stress level indicates that the effect from powder shape is relatively minor.

## 4. Discussion

### 4.1. Powder consolidation models

To assess the effect of creep and transformation-mismatch plasticity on Ti–6Al–4V powder densification, the densification curves are modeled with continuum models derived for creep densification by Arzt et al. [26], used by others [4,27–30] for creep densification, and extended by Schuh et al. [4] for densification of CP-Ti under transformation-mismatch plasticity conditions.

The uniaxial constitutive equations for bulk material, deforming under uniaxial stress $\sigma_x$ for conditions of transformation-mismatch plasticity [11] and creep, are given respectively as:

$$\bar{\dot{\varepsilon}}_x = \frac{4}{3} \cdot \frac{5 \cdot n}{4 \cdot n + 1} \cdot \frac{\Delta V}{V} \cdot \frac{1}{\Delta t} \cdot \frac{\sigma_x}{\sigma_0} \tag{1}$$

$$\dot{\varepsilon}_x = C \cdot \sigma_x^n \tag{2}$$

where $\bar{\dot{\varepsilon}}_x$ is the average uniaxial strain rate during thermal-cycling transformation-mismatch plasticity, $\dot{\varepsilon}_x$ is the steady-state (secondary) uniaxial strain rate due to isothermal creep, $n$ is the creep stress exponent ($n = 2.8$ for Ti–6Al–4V [8]), $\Delta V/V$ is the volume mismatch between the allotropic $\alpha$ and $\beta$ phases, $\Delta t$ is the period of the thermal cycles ($\Delta t = 191$ s) spanning two transformations (heating and cooling), $\sigma_0$ is the average internal stress generated during the phase transformation ($\sigma_0 = 7.4$ MPa for Ti–6Al–4V [12]) and $C$ is a constant incorporating an Arrhenius temperature dependence ($C = 4.8 \times 10^{-7}$ MPa$^{-2.8}$ s$^{-1}$ for Ti–6Al–4V at 1020 °C [8,12]). Although the effective volume mismatch can in principle be determined from Ref. [12], where the $\beta$-volume fraction and volume mismatch measured were measured as a function of temperature via X-ray diffraction, it is more direct to use the effective volume mismatch measured by transformation-mismatch plasticity of Ti–6Al–4V under cycling conditions similar to those used here for densification. From the strain increment $\Delta\varepsilon$ measured in a study [12] where Ti–6Al–4V samples were deformed under tension for various temperature amplitudes shown in Fig. 8, the effective volume mismatch $\Delta V/V$ is calculated from Eq. (1) as 0.96% for thermal cycling of Ti–6Al–4V between 860 and 1020 °C.

In a densifying powder compact in the initial stage of consolidation ($\rho < 90\%$), the effective interparticle contact pressure $\sigma_e$ is given by [4,26]:

$$\sigma_e = B_i \cdot \frac{(1 - \rho_0)}{\rho^2 \cdot (\rho - \rho_0)} \cdot \sigma \tag{3}$$

where $\sigma$ is the uniaxial stress (pressure) applied on the die piston, $B_i = 1.1$ is a dimensionless constant taking into
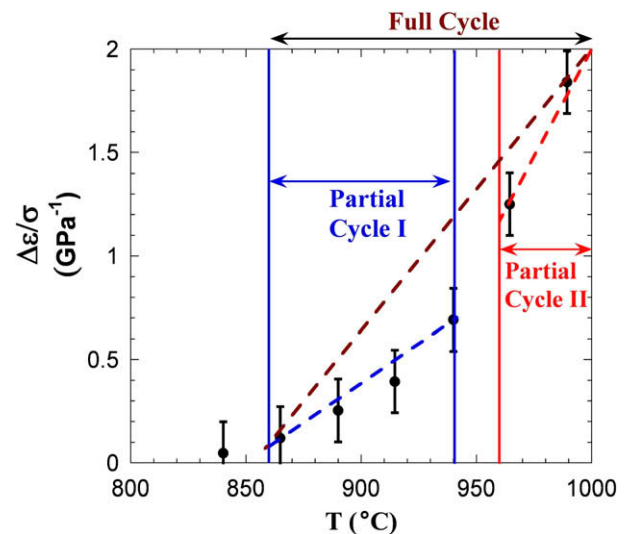


Fig. 8. Plot of strain increment per thermal cycle (divided by applied stress of 1.95 MPa) vs. upper cycling temperature (with lower temperature of 840 °C) for uniaxial tensile tests on dense Ti–6Al–4V. Data are from Ref. [12] and partial cycling ranges are shown with arrows.

account compaction geometry, $\rho$ is the compact relative density and $\rho_0$ its initial relative density.

The densification rate $\dot{\rho}$ for creep conditions can then be expressed as [4,26]:

$$\dot{\rho} = 3.06 \cdot C \cdot \left(\frac{1-\rho_0}{\rho-\rho_0}\right)^{n-1/2} \frac{\rho_0^{1/3}}{\rho^{2n-2/3}} \cdot \left(\frac{B_i \cdot \sigma}{3}\right)^n \qquad (4)$$

Under thermal cycling conditions where transformation-mismatch plasticity (Eq. (1)) rather than isothermal creep (Eq. (2)) is the dominant deformation mechanism, the densification rate is given as [4]:

$$\dot{\rho} = 1.36 \cdot \frac{5 \cdot n}{4 \cdot n + 1} \cdot \frac{\Delta V}{V} \cdot \frac{1}{\Delta t} \cdot \left(\frac{1-\rho_0}{\rho-\rho_0}\right)^{1/2} \cdot \frac{\rho_0^{1/3}}{\rho^{4/3}} \cdot \frac{B_i \cdot \sigma}{\sigma_0} \qquad (5)$$

Eqs. (4) and (5) are numerically integrated to find $\rho(t)$, for a given initial density $\rho_0$, which can then be directly compared with experimental $\rho(t)$ densification curves.

For final stage consolidation ($90\% < \rho < 100\%$), the densification rate due to creep is given as [4,26]:

$$\dot{\rho} = \frac{3}{2} \cdot C \cdot \frac{\rho \cdot (1-\rho)}{(1-(1-\rho)^{1/n})^n} \cdot \left(\frac{3B_f \sigma}{2 \cdot n}\right)^n \qquad (6)$$

and that due to transformation-mismatch plasticity by Schuh et al. [4]:

$$\dot{\rho} = 3 \cdot \frac{5 \cdot n}{4 \cdot n + 1} \cdot \frac{\Delta V}{V} \cdot \frac{1}{\Delta t} \cdot (1-\rho) \cdot \left(\frac{B_f \sigma}{\sigma_0}\right)^2 \qquad (7)$$

where the dimensionless constant $B_f = 1.8$ takes into account the non-isostatic stress state around isolated cavities shrinking under the influence of the applied stress. Similarly, Eqs. (6) and (7) are numerically integrated for final stage densification to compare with experimental densification curves.

### 4.2. Comparison between experiments and models

#### 4.2.1. Thermal cycling densification

Fig. 9a–d compares, for four different stresses, the predicted densification curves under thermal cycling condi-
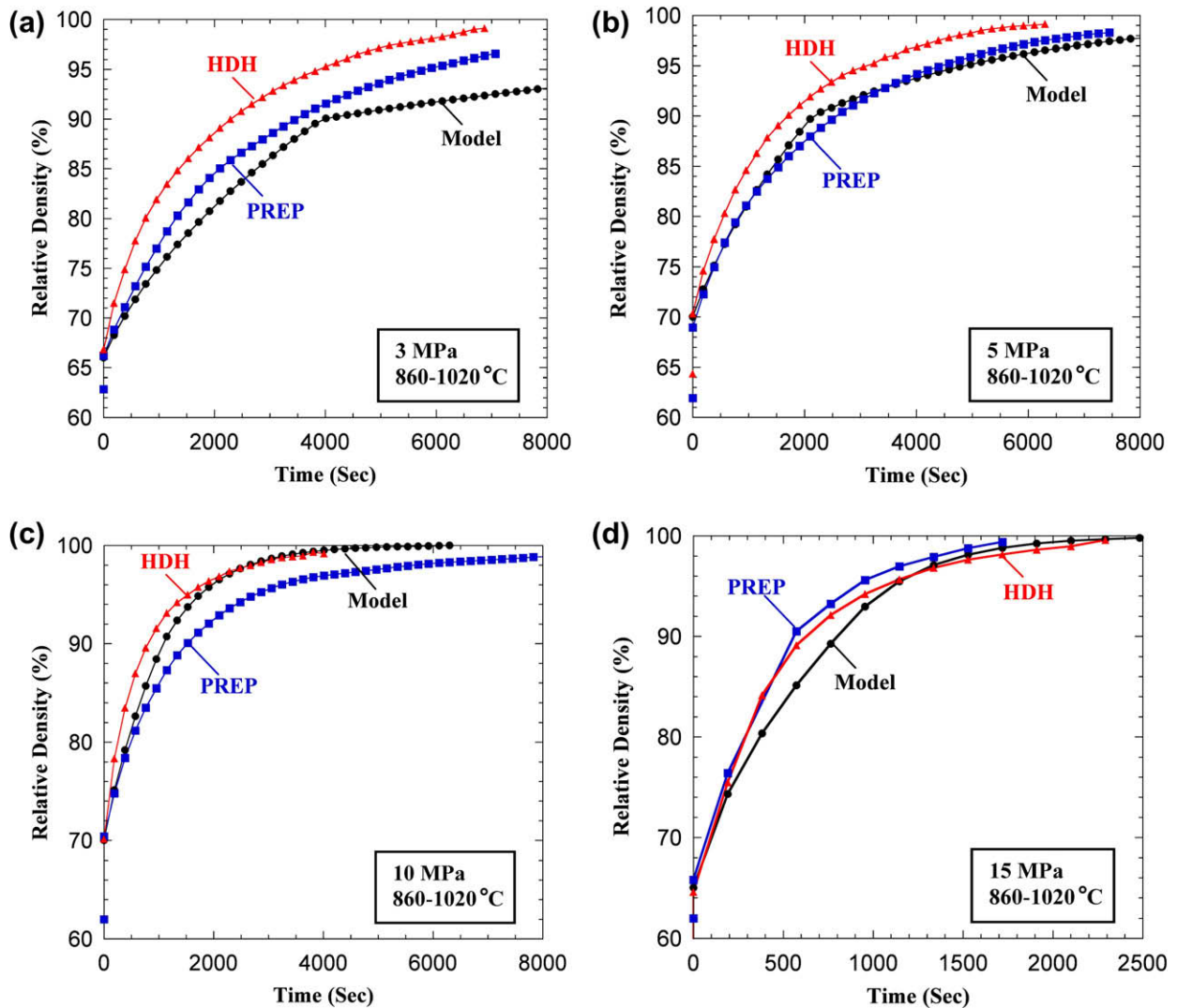


Fig. 9. Densification curves for thermal cycling conditions, as measured experimentally for PREP and HDH powders and as predicted from models for: (a) 3 MPa, (b) 5 MPa, (c) 10 MPa and (d) 15 MPa.

tions, with both the initial densification stage (Eq. (5)) and the final stage (Eq. (7)), with the respective experimental densification curves for both types of powders (Fig. 7a and b). To allow comparison, the experimental curves are shifted along the x-axis so their relative density at time $t = 0$ is between 0.65 and 0.70 as initial density, corresponding to the value reached immediately after applying the densifying load. This relative density is experimentally achieved very rapidly after applying the uniaxial stress, regardless of powder shape. The agreement between the model predictions and the experimental densification curves is generally satisfactory given the simplifications in the model, the lack of adjustable parameters, the fact that Eq. (1) is valid only at small stresses and the imperfect reproducibility of the experimental curves. At the three lowest applied stresses, densification of the PREP powders is somewhat slower than for the HDH powders. This may be due to the higher stress concentration, at low relative density, at the point of contacts between angular powders, as compared to spherical powders.

Powder densification under partial thermal cycling, with experimental data shown in Fig. 6b, can be predicted with models for full thermal cycling (Eqs. (5) and (7)) provided the effective volume mismatch is adjusted for the partial phase transformation. As shown in Fig. 8, the effective volume mismatch $\Delta V/V$ of 0.96% for the full transformation of Ti–6Al–4V is reduced to 0.27% for the low-temperature thermal cycling (860–940 °C) and 0.41% for the high temperature cycling (960–1020 °C). The densification behavior at 10 MPa predicted for both partial thermal cycling and the full thermal cycling is shown in Fig. 10, and is in general agreement with experimental densification curves shown in Fig. 6b. In particular, both experiments and models indicate that partial thermal cycling between 960 and 1020 °C provides densification kinetics nearly as rapid as full cycling (860–1020 °C), because the temperature depen-

dence of the volume mismatch is highest near the transus temperature (995 ± 15 °C [25]), as shown in Fig. 8. Considering the volume fraction effect of the α–β phase, the lower effective volume mismatch change can be compensated by faster thermal cycling rate at the same induction power input.

### 4.2.2. Isothermal densification

The calculated and experimental densification curves are compared in Fig. 11a and b for applied stresses of 5 and 10 MPa, respectively. Agreement between experimental and predicted curves is reasonable, given the model's simplifying assumption and lack of adjustable parameters, the uncertainty on the stress exponent $n = 2.8$ (which affects strongly the densification rate), and the experimental error between curves illustrated in Fig. 6a. At the lower stress level of 5 MPa, furthermore, it is possible that diffusional creep is active as deformation mechanism, thus
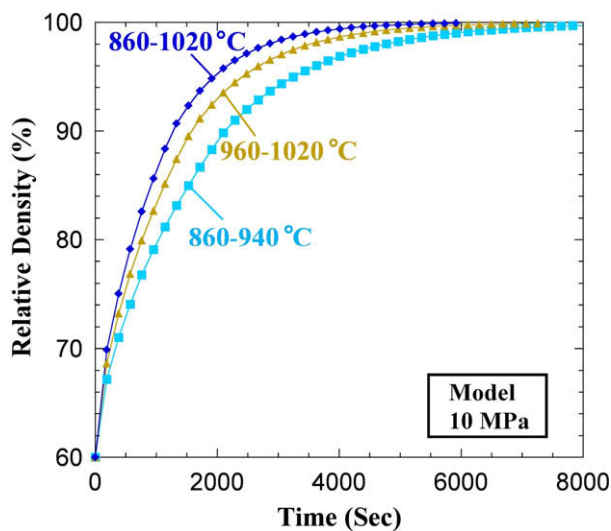


Fig. 10. Densification curves calculated from model for full or partial thermal cycling (constant stress of 10 MPa).
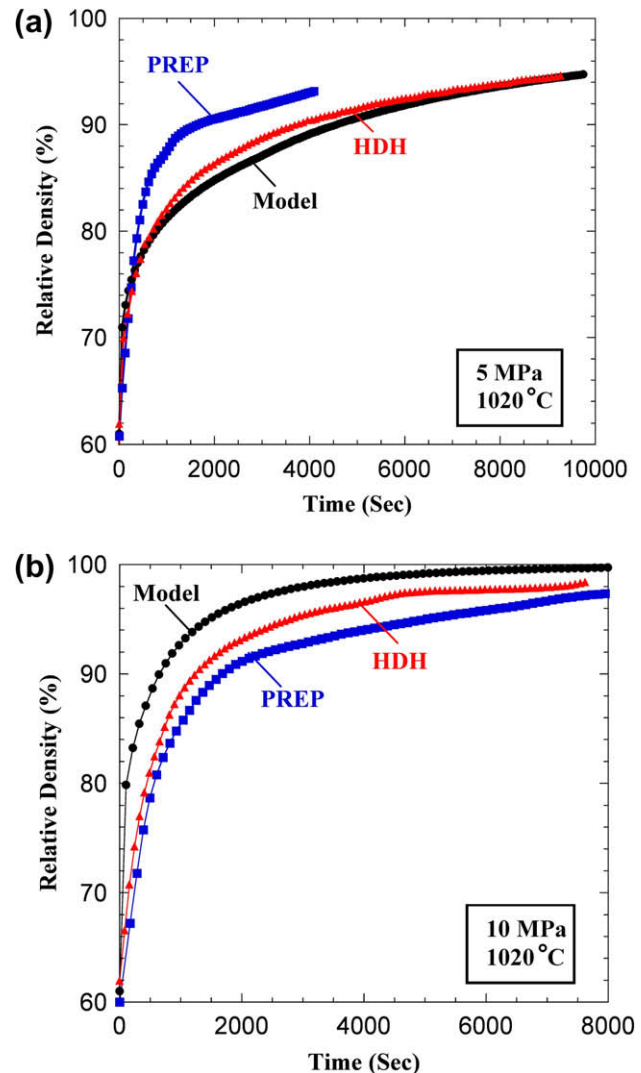


Fig. 11. Densification curves for isothermal conditions (1020 °C), as measured experimentally for PREP and HDH powders and as predicted from model for: (a) 5 MPa and (b) 10 MPa.

enhancing the densification as compared to predictions which assume that only dislocation creep (Eq. (2)) is active as a deformation mechanism.

Both experiments and modeling indicate that transformation-mismatch plasticity accelerates markedly the kinetics of Ti–6Al–4V powder densification. This opens the door for powder densification at stresses and average temperatures significantly lower than for the traditional HIP powder densification method, while also allowing the use of dies to create complex shapes.

## 5. Conclusions

Densification kinetics during uniaxial die pressing of Ti–6Al–4V powders were measured under thermal cycling (860–1020 °C) or isothermal (1020 °C) conditions for applied stresses ranging from 3 to 30 MPa. Densification kinetics are affected weakly by powder shape (rounded vs. angular) but are markedly enhanced by transformation-mismatch plasticity operating during thermal cycling. Cycling allows full density to be reached in a few hours for stresses as low as 10 MPa, with tensile properties of the densified specimen similar to those reported for HIP-densified powders at much higher pressures. Reduction of the temperature range produces less densification per cycle, but nearly the same average densification rate, because the cycling rate is increased. The kinetics of thermal cycling and isothermal densification are successfully modeled based on creep and transformation-mismatch plasticity, respectively.

## Acknowledgements

## References

[1] Froes F, Mashl S, Hebeisen J, Moxson V, Duz V. JOM J Miner, Met Mater Soc 2004;56:46.
[2] Taylor N, Dunand DC, Mortensen A. Acta Metall Mater 1993;41:955.
[3] Dunand D, Zwigl P. Metall Mater Trans A 2001;32:841.
[4] Schuh C, Noel P, Dunand DC. Acta Mater 2000;48:1639.
[5] Zwigl P, Dunand DC. Acta Mater 1997;45:5285.
[6] Dunand DC, Bedell CM. Acta Mater 1996;44:1063.
[7] Choe H, Schuh CA, Dunand DC. J Appl Phys 2008;103:103518.
[8] Li Q, Chen E, Bice D, Dunand DC. Metall Mater Trans A 2007;38:44.
[9] Zwigl P, Dunand DC. J Mater Process Technol 2001;117:409.
[10] Schuh CA. Philos Mag A 2002;82:2441.
[11] Greenwood GW, Johnson RH. Proc Roy Soc Lond. Ser A, Math Phys Sci 1965;283:403.
[12] Schuh C, Dunand DC. Acta Mater 2001;49:199.
[13] Schuh C, Dunand DC. J Mater Res 2001;16:865.
[14] Dunand DC, Myojin S. Mater Sci Eng A 1997;230:25.
[15] Schuh C, Dunand DC. Scripta Mater 2001;45:631.
[16] Schuh C, Dunand DC. Int J Plast 2001;17:317.
[17] Frary M, Schuh C, Dunand DC. Metall Mater Trans A 2002;33:1669.
[18] Murray NGD, Dunand DC. Acta Mater 2004;52:2279.
[19] Murray NGD, Schuh CA, Dunand DC. Scripta Mater 2003;49:879.
[20] Shen H, Oppenheimer SM, Dunand DC, Brinson LC. Mech Mater 2006;38:933.
[21] Ruano O, Eiselstein L, Sherby O. Metall Mater Trans A 1982;13:1785.
[22] Oshida Y. J Jpn Soc Powder Metall 1975;22:147.
[23] Ruano O, Wadsworth J, Sherby O. Metall Mater Trans A 1982;13:355.
[24] Leriche D, Gautier E, Simon A. In: Lacombe P, Tricot R, Beranger G, editors. Proceedings of the sixth world conference on titanium. Cannes: Ed de Physique; 1988. p. 163.
[25] Boyer R, Welsch G, Collings EW, editors. Materials properties handbook: titanium alloys. Materials Park (OH): ASM International; 1994.
[26] Arzt E, Ashby M, Easterling K. Metall Mater Trans A 1983;14:211.
[27] Wilkinson DS, Ashby MF. Acta Metall 1975;23:1277.
[28] Helle AS, Easterling KE, Ashby MF. Acta Metall 1985;33:2163.
[29] Liu Y-M, Wadley HNG, Duva JM. Acta Metall Mater 1994;42:2247.
[30] Duva JM, Crow PD. Acta Metall Mater 1992;40:31.